

EXTRACTION, CHARACTERIZATION AND KINETICS OF THERMAL DECOMPOSITION OF LIGNIN FROM DATE SEEDS USING MODEL-FREE AND FITTING APPROACHES

NIDHOIM ASSOUMANI,* MARYAM EL MAROUANI,** LAHCEN EL HAMD AOUI,**
LÁSZLO TRIF,**** FATIMA KIFANI-SAHBAN* and MERLIN SIMO-TAGNE*****

**Team of Modeling and Simulation in Mechanics and Energetic, Physical Department,
Faculty of Sciences, Mohammed V University in Rabat, Rabat, Morocco*

***Department of Chemistry, Affiliated Colleges, Hafr Al-Batin University, Kingdom of Saudi Arabia*

****Laboratory of Materials, Nanotechnology and Environment, Department of Chemistry,
Faculty of Sciences, Mohammed V University in Rabat, Rabat, Morocco*

*****Institute of Materials and Environmental Chemistry, Research Center for Natural Sciences,
Magyar Tudósok Körútja, 2, Hungary*

******CFA-CFPPA of Mirecourt, 22 rue du Docteur Grosjean, 88500 Mirecourt, France*

✉ *Corresponding author: L. El Hamdaoui, la.elhamdaoui@gmail.com*

Received April 15, 2023

Lignin is known to have great potential for use as a renewable feedstock in a variety of industrial applications, including energy and chemicals. Furthermore, to ensure an efficient valorization of lignin, the efficiency of the isolation procedure and the knowledge of its properties are crucial. In the present study, we extracted lignin from date seeds using the Klason method. The extracted lignin was characterized by FT-IR spectrometry, XRD and SEM-EDX analysis. The thermal behavior of date seeds lignin has been investigated using TGA and DSC. Several isoconversional and model-fitting methods were employed to derive the kinetic parameters. A comparison between these procedures was carried out. Based on the results of activation energy (E_a) and pre-exponential factor (A) determined using Kissinger's equation for date seeds lignin decomposition, some thermodynamic parameters (ΔS^\ddagger , ΔH^\ddagger and ΔG^\ddagger) were determined. Following a broad endothermic stage, a large exothermic peak was observed in the DSC plots, attesting to the overall exothermicity of the lignin pyrolysis. From the derivative curve of DSC plots, the glass transition temperature T_g of the studied lignin was determined. High values of T_g , ranging from 102.62 to 127.28 °C, significantly affected by the heating rate, were found.

Keywords: lignin extraction, DSC, TGA, model fitting methods, kinetics

INTRODUCTION

Due to the unbridled consumption of fossil fuels and their depletion, among other reasons, in-depth research on the use of non-conventional energy sources is gaining more and more interest. Among these sources, biomass, in particular lignocellulosic biomass, is a source rich in energy, widely available and renewable, and therefore, likely to replace, in the long term, conventional energy sources.¹ The three main natural polymers that make up lignocellulosic biomass are cellulose, lignin, and hemicelluloses. Hemicelluloses and lignin form covalent bonds with each other, but cellulose forms hydrogen bonds with both. The three main elements are

clearly separate from one another. Unlike cellulose and hemicelluloses, which are both carbohydrates, lignin is an aromatic polymer. Lignin is the second most abundant natural material among these three components, accounting for 10–30% of lignocellulosic biomass.^{2,3} It is the “glue” that connects cellulose and hemicelluloses in the woody material; it is insoluble in water and in the conventional organic solvents and stable in nature. At the structural level, lignin is a three-dimensional, highly cross-linked biopolymer that arises from enzymatic polymerization of different types of substituted phenols, namely p-coumaryl, coniferyl, and

sinapyl alcohols, forming a vast number of functional groups and a complex structure.^{4,6} The physical and chemical characteristics of lignin will differ depending on its source and the extraction method used.

Lignin has recently been discovered to be a significant source of chemicals and energy.^{7,8} Many applications have involved it, ranging from dyes, emulsifiers, synthetic paints, fuels, floors, binding, thermosets, and dispersion agents to roadway treatments.^{9,10}

Morocco is a producer of dates and date-based products. Since the establishment of the Green Morocco Plan in recent years, the output of dates has increased satisfactorily. As a result, the increased production of dates favors a plethora of by-products related to the packing and processing of items produced from date seeds. The latter, which was previously utilized as cattle fodder, has recently been valorized and sold in small-scale cooperatives as coffee and oil.

In previous research,¹¹ the physicochemical properties of date seeds from the variety "Boufagouss", as well as their thermal properties in chemical regime and fixed bed conditions, have been investigated. In this paper, we propose to investigate the physical and chemical characteristics of lignin extracted from date seeds of the mentioned variety. As a result, this work aspires to contribute to the valorization of date seeds. Understanding the kinetics of lignin pyrolysis is essential for better understanding the processes involved and more effectively optimizing the pyrolysis process to obtain the desired products. However, the literature is much scarcer on the properties of lignin extracted from seed feedstocks, which are very abundant waste products – therefore, this has been set as the focus of our study. Previously, several research groups have shown that differences in lignin sources, chemical structures, lignin isolation methods, and various calculation methodologies may explain the wide range of reported kinetic parameters. For example, Domínguez *et al.*¹² observed first order degradation, using a model fitting, on an Olganosolv lignin (*Eucalyptus*), to obtain an activation energy of 19.1–42.5 kJ/mol over a temperature range of 30–900 °C, whereas Ferdous *et al.*¹³ used the distributed activation energy model (DAEM) (reactions are assumed to consist of a set of irreversible first-order reactions that have different activation energies) to calculate the activation energy of Alcell and Kraft lignins as

129 to 361 kJ/mol over a temperature range of 80–800 °C.

The literature on lignin extraction shows a variety of methods used; in the current study, lignin was isolated from date seeds using the Klason lignin method. The extracted lignin sample was analyzed after impurities were removed by FT-IR spectroscopy and X-ray diffraction (XRD). Thermogravimetric analysis (TGA) and differential scanning calorimetry (DSC) were used to determine the degradation of lignin and the char content by measuring mass loss depending on the temperature. The morphology and microstructure of this biomaterial were examined using SEM microscopy.

EXPERIMENTAL

Material

Klason lignin was extracted from date seeds collected in a field near Rabat, Morocco. The raw material was ground to powder using a microgrinder. Afterwards, extraction was performed in a Soxhlet apparatus for 4 hours with 20 g of this powder and an ethanol-toluene mixture (1:2 v/v).

At room temperature, the residue was hydrolyzed with 72% sulfuric acid and continuously stirred for 2 hours. After that, the sulfuric acid was diluted to 3% and the mixture was refluxed for 2 hours before the insoluble residue was filtered, washed, dried, and weighed as Klason lignin.^{14,15}

All of the chemicals used in the Klason lignin extraction were purchased from Sigma Aldrich, including toluene (C₇H₈), ethanol (C₂H₅OH), and sulfuric acid (H₂SO₄). All reagents were used without additional purification, and all experiments were carried out with twice-distilled water. The obtained yield of lignin was about 30%.

Methods of material analysis

FT-IR spectroscopic characterization of Klason lignin

A Shimadzu FTIR-8400s, fitted with MIRacle™ ATR attachment, was used to obtain FT-IR data of the extracted lignin sample. A resolution of 4 cm⁻¹ was used, and 50 scans between 500 and 4000 cm⁻¹ were recorded.

X-ray diffraction

X-ray diffraction is an efficient method for examining the crystallinity, amorphous and structural characteristics of bio-based polymers. A powder diffractometer, model Lab XRD-6100 Shimadzu, using a monochromatic Cu K (1.5418 Å) X-ray source and a voltage of 50 kV, was used to produce the spectra of the lignin sample at room temperature. An angular range of 5 to 35°, a step size of 0.02°, and a scanning

time of 2 seconds per step was used in the analysis of the lignin sample in continuous mode.

Thermogravimetric and differential scanning calorimetric analyses

The thermogravimetric (TG) and differential scanning calorimetric (DSC) measurements of the lignin samples were carried out on a Setaram Labsys Evo (Lyon, France) thermal analyzer in flowing (flow rate of 90 mL/min) high purity (99.999%) nitrogen. The samples were used as received, and were weighed before the measurements in 100 μ L Al_2O_3 crucibles. The samples were heated from 25 to 600 $^\circ\text{C}$ with 4 different rates (5, 10, 15, and 20 $^\circ\text{C}/\text{min}$). The obtained data were baseline corrected and further processed with the thermoanalyzer's processing software (Calisto Processing, ver. 2.06). The thermal analyzer (both the temperature scale and calorimetric sensitivity) was calibrated by a multipoint calibration method, in which seven different certified reference materials (CRM's) were used to cover the thermal analyzer's entire operating temperature range. The initial sample mass was around 8 mg, with a particle size of 180 μm . To minimize experimental uncertainties, three replicates were used for thermogravimetric analyses.

The equipment was set to the following parameters: temperature accuracy ($^\circ\text{C}$) $\pm 0.05^*$, temperature precision ($^\circ\text{C}$) ± 0.15 ; enthalpy accuracy (%) ± 0.8 ; calorimetric precision (%) ± 0.4 ; RMS noise (μW) 0.2; resolution (μW) 0.35; 0.035; dynamic range (mW) ± 290 ; ± 2900 ; weighing precision $\pm 0.01\%$ TG; resolution 0.2 $\mu\text{g}/0.02 \mu\text{g}$; baseline dynamic drift (one hour) 10 μg ; TG reproducibility up to 1 200 $^\circ\text{C} < 50 \mu\text{g}$.

Scanning electron microscopy (SEM) analyses

The surface morphology of the lignin biomaterial was analyzed using an FEI Quanta 200 electron microscope. The samples were evaluated at a 30 kV accelerating voltage after being coated with a coating of carbon to improve their conductivity.

Kinetic approach

Theoretical background

The conversion α is generally used to explain the progression of the solid-state reaction. It is mathematically expressed using thermogravimetric data as follows:

$$\alpha = \frac{m_0 - m_t}{m_0 - m_f} \quad (1)$$

where m_t , m_0 and m_f are the mass at time t , initial mass, and final mass, respectively, and they are all taken from the findings of the experiment on mass loss of the sample. The kinetic equation of the reaction can then be generalized by the formula:

$$\frac{d\alpha}{dt} = k(T)f(\alpha) \quad (2)$$

where $\frac{d\alpha}{dt}$ is the mass conversion rate, T is the absolute temperature (K), $k(T)$ is the degradation rate constant, and $f(\alpha)$ represents the differential degradation mode. The rate constant $k(T)$ is a function of temperature and is usually described by the Arrhenius relationship:

$$k(T) = A \exp\left(-\frac{E}{RT}\right) \quad (3)$$

where E , A and R are the apparent activation energy, the pre-exponential factor, and the gas constant, respectively. When the reaction proceeds under non-isothermal conditions, with a constant temperature rise rate $\beta = dT/dt$, Equation (2) can be written as follows:

$$\frac{d\alpha}{dt} = \beta \frac{d\alpha}{dT} = Af(\alpha) \exp\left(-\frac{E}{RT}\right) \quad (4)$$

The fraction of material used over time under non-isothermal conditions is expressed by this equation.

After variable separation and integration, while accounting for temperature variation as a function of time and assuming independence of the pre-exponential factor A with respect to temperature, Equation (4) may be transformed as:

$$g(\alpha) = \int_0^\alpha \frac{d\alpha}{f(\alpha)} = \frac{A}{\beta} \int_{T_0}^T \exp\left(-\frac{E}{RT}\right) dT \quad (5)$$

where $g(\alpha)$ represents the integral degradation mode and T_0 the initial temperature. The right-hand side of Equation (5) is a temperature-dependent integral function with no analytical solution that can be determined using either approximations or numerical integration. Non-isothermal TGA was used in this study to obtain the activation energy. Model-free and model fitting non-isothermal approaches, which demand a series of experimental experiments at various heating rates, were used to determine kinetic parameters.

Kinetic analysis methods

Model-free approaches are thought to be the most accurate ways to determine the activation energy, therefore the ICTAC kinetics committee advises using model-free (isoconversional) methodology for kinetically analyzing non-isothermal studies.¹⁶ Without making any modelistic assumptions, model-free methods can determine the activation energy, E_a , at successive conversion levels. The activation energy at a specific degree of conversion is independent of the heating rate using isoconversional methods. To unravel the kinetics of thermal degradation processes, isoconversional approaches based on numerous heating programs are now the most often used approach.

Using several temperature integral approaches and the first-order reaction assumption, the kinetic parameters, such as E and $\ln A$ were obtained from the non-isothermal mass loss data. In-depth comparisons

have been made between the isoconversional results of Friedman,¹⁷ Flynn–Wall–Ozawa method,^{18,19} Kissinger–Akahira–Sunose,^{20,21} Coats–Redfern method,²² Madhusudanan–Krishnan–Ninan

approximation method,²³ Tang method²⁴ and Kissinger.²⁰

The mathematical expression of each method is shown in Table 1.

Table 1
Kinetic analysis methods

Friedman method ¹⁷ (Fr)	$\text{Ln}\left(\frac{d\alpha}{dt}\right) = \text{Ln}[Af(\alpha)] - \frac{E_a}{RT}$	(6)
Kissinger-Akahira-Sunose method ^{20,21} (KAS)	$\text{Ln}\left(\frac{\beta}{T^2}\right) = \text{Ln}\left(\frac{AR}{E_a g(\alpha)}\right) - \frac{E_a}{RT}$	(7)
Kissinger method ²⁰	$\text{Ln}\left(\frac{\beta}{T_m^2}\right) = \text{Ln}\left(\frac{AR}{E_a}\right) - \frac{E_a}{RT_m}$	(8)
Flynn–Wall–Ozawa method ^{18,19} (FWO)	$\text{Ln}(\beta) = \text{Ln}\left(\frac{AE_a}{Rg(\alpha)}\right) - 5,331 - 1,052 \frac{E_a}{RT}$	(9)
Madhusudanan–Krishnan–Ninan method ²³ (MKN)	$\text{Ln}\left[\frac{\beta}{T^{1.884318}}\right] = \text{Ln}\left[\frac{A}{g(\alpha)}\left(\frac{E_a}{R}\right)^{-0.884318}\right] - 0,389677 - 1,0011928 \frac{E_a}{RT}$	(10)
Tang method ²⁴	$\text{Ln}\left[\frac{\beta}{T^{1.894661}}\right] = \text{Ln}\left[\frac{A}{g(\alpha)}\left(\frac{E_a}{R}\right)^{-0.894661}\right] - 0,37773896 - 1,00145033 \frac{E_a}{RT}$	(11)
Coats–Redfern method ²² (CR)	$\text{Ln}\left(\frac{g(\alpha)}{T^2}\right) = \text{Ln}\left(\frac{AR}{\beta E_a}\right) - \frac{E_a}{RT}$	(12)

The kinetic parameters, especially E_a and A , can be obtained from the plot of the curves $\text{Ln}\left(\frac{d\alpha}{dt}\right)$, $\text{Ln}\left(\frac{\beta}{T^2}\right)$, $\text{Ln}\left(\frac{\beta}{T_m^2}\right)$, $\text{Ln}(\beta)$, $\text{Ln}\left[\frac{\beta}{T^{1.884318}}\right]$, $\text{Ln}\left[\frac{\beta}{T^{1.894661}}\right]$ and $\text{Ln}\left(\frac{g(\alpha)}{T^2}\right)$ versus $1/T$, respectively, by the methods of Friedman, KAS, FWO, MKN, Tang and Coats-Redfern.

Criado method

The Criado method²⁵ can be used to derive the kinetic model of the process if the activation energy value is known. Equation (4) and Equation (12) are combined to create the following equation:

$$\frac{Z(x)}{Z(0.5)} = \frac{f(\alpha)g(\alpha)}{f(0.5)g(0.5)} = \left(\frac{T_x}{T_{0.5}}\right)^2 \frac{(dx/dt)_x}{(dx/dt)_{0.5}} \quad (13)$$

where 0.5 indicates to the conversion in $x = 0.5$.

The left side of Equation (13), $(f(\alpha)g(\alpha))/(f(0.5)g(0.5))$, is a reduced theoretical curve that represents each reaction process, the experimental data can be used to determine the right side of the equation that represents the reduced rate.

Calculation of thermodynamic parameters

Based on the transition state theory, the rate constant of the process can be given as the Eyring equation of the activated complex:^{26,27}

$$k(T) = \frac{\chi e k_B T_p}{h} \exp\left(\frac{\Delta S^\#}{R}\right) \exp\left(-\frac{E_a}{RT}\right) \quad (14)$$

where χ is transmission coefficient, k_B is Boltzmann’s constant, h is Planck’s constant and $e = 2.7183$ is Neper’s number and T_p is the DTG curves’ typical peak temperature when heated at various rates.

Considering that:

$$A = \frac{\chi e k_B T_p}{h} \exp\left(\frac{\Delta S^\#}{R}\right) \quad (15)$$

Calculations of the thermodynamic functions, such as $\Delta S^\#$, $\Delta H^\#$ and $\Delta G^\#$, that accurately describe the decomposition process are feasible.²⁷ Then, the following formulas may be used to compute the changes in entropy and enthalpy:

$$\Delta S^\# = R \text{Ln}\left(\frac{Ah}{\chi e k_B T_p}\right) \quad (16)$$

$$\Delta H^\# = E_a - RT_p \quad (17)$$

The change of Gibbs free energy $\Delta G^\#$ can be determined from the well-known thermodynamic formula:

$$\Delta G^\# = \Delta H^\# - T_p \Delta S^\# \quad (18)$$

The values of $\Delta S^\#$, $\Delta H^\#$ and $\Delta G^\#$ were calculated at $T = T_p$, since this temperature characterizes the highest rate of the process.

Based on the results of E_a and A calculated from Kissinger’s equation over the whole DSL decomposition, $\Delta S^\#$, $\Delta H^\#$ and $\Delta G^\#$ can be obtained for the formation of the activated complex from the reagent.

RESULTS AND DISCUSSION

FT-IR spectroscopic characterization of lignin

The IR spectrum of Klason lignin extracted from date seeds clearly indicated the existence of different functional groups characteristic of the lignin material, such as the O-H group, aromatic skeletal vibrations, aromatic C-H, carbonyl and carboxyl groups. The IR spectrum of DSL (Fig. 1) shows a strong broad overlapping band between 3685 and 3027 cm^{-1} , centered at 3380 cm^{-1} , which is ascribed to O-H stretching vibration $\nu(\text{O-H})$ in alcoholic and phenolic hydroxyl groups.²⁸⁻³⁰ The band at 2923 cm^{-1} is assigned to the methyl and methylene group, the sharp peak at 2849 cm^{-1} corresponds to the stretching vibrations $\nu(\text{C-H})$ in CH_3 of the methoxyl group. Also, a small peak is noted at 1705 cm^{-1} , attributed to carbonyl groups and carbonyl stretching unconjugated ketones.³⁰⁻³² Meanwhile, the skeletal ($\text{C}=\text{C}$) vibrations in aromatic rings are located at 1556 cm^{-1} , the stretching vibration for ($\text{C}=\text{C}$) in aliphatic chains creates the shoulder at around 1656 cm^{-1} ,³³⁻³⁵ and a positive peak at 1462 cm^{-1} assigned to $-\text{CH}$ deformations in $-\text{CH}_3$ and $-\text{CH}_2$. The thin absorption with medium intensity detected at about 1394 cm^{-1} is attributed to the vibration of deformation in plane $\delta(\text{O-H})$ of phenols.³⁰⁻³²

The sharp peak at 1214 cm^{-1} is ascribed to syringyl ring breathing with CO stretching. The peaks at 1040 and at 739 cm^{-1} represent aromatic C-H in-plane deformation and out-of-plane deformation, respectively. The existence of out-of-plane deformation $\gamma(\text{O-H})$ of primary and secondary aliphatic hydroxyl groups and/or phenolic hydroxyl groups is demonstrated by the narrow and weak band at 692 cm^{-1} .

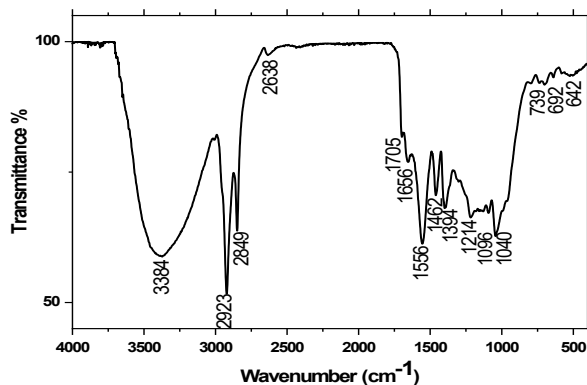


Figure 1: FT-IR spectrum of Klason lignin extracted from date seeds (DSL)

X-ray diffraction study (XRD)

X-ray diffraction analysis was carried out to examine the lignin surface from a morphological point of view in more detail. The XRD diffractogram of lignin is shown in Figure 2, it shows a broad peak of amorphous halo, with a maximum centered at $2\theta = 21.98^\circ$, which confirms that chitosan is naturally amorphous. In the literature, several researchers have demonstrated that the differences in the lignin sources, chemical structures, and isolation methods may explain the difference observed for the amorphous peak of lignin samples, for example, Goudarzi *et al.*³⁶ and Kubo *et al.*³⁷ observed an average peak for hardwood, centered at $21.2 \pm 0.15^\circ$ and at 22.7° , respectively.

Surface morphology

The surface phenomena of lignin extracted from date seeds were observed by an electron microscope scanning with an EDX attachment. SEM images of the surface morphology of the studied lignin were acquired at various magnifications: $\times 100$ (a), $\times 250$ (b), and $\times 1000$ (c), and shown in Figure 3. The lignin is revealed to have a granular appearance, with grains of varied sizes and compact structures that formed platelet aggregation. It also reveals certain areas that appear to be occupied by bubbles. Moreover, the surface of the lignin shows microcavities.

EDX examination of this biomaterial (Fig. 4) reveals the presence of important elements, such as carbon (C 53.54%) and oxygen (O 45.77%), as well as minor amounts of minerals.

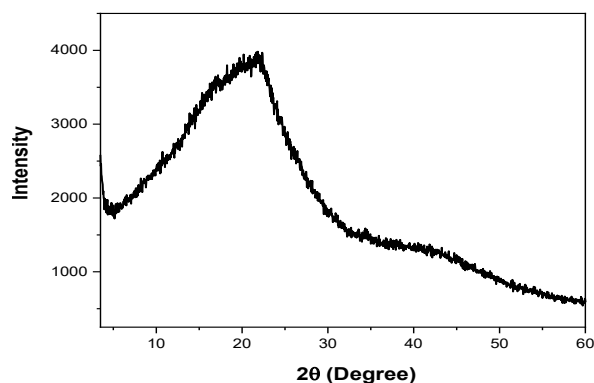


Figure 2: XRD pattern for lignin extracted from date seeds

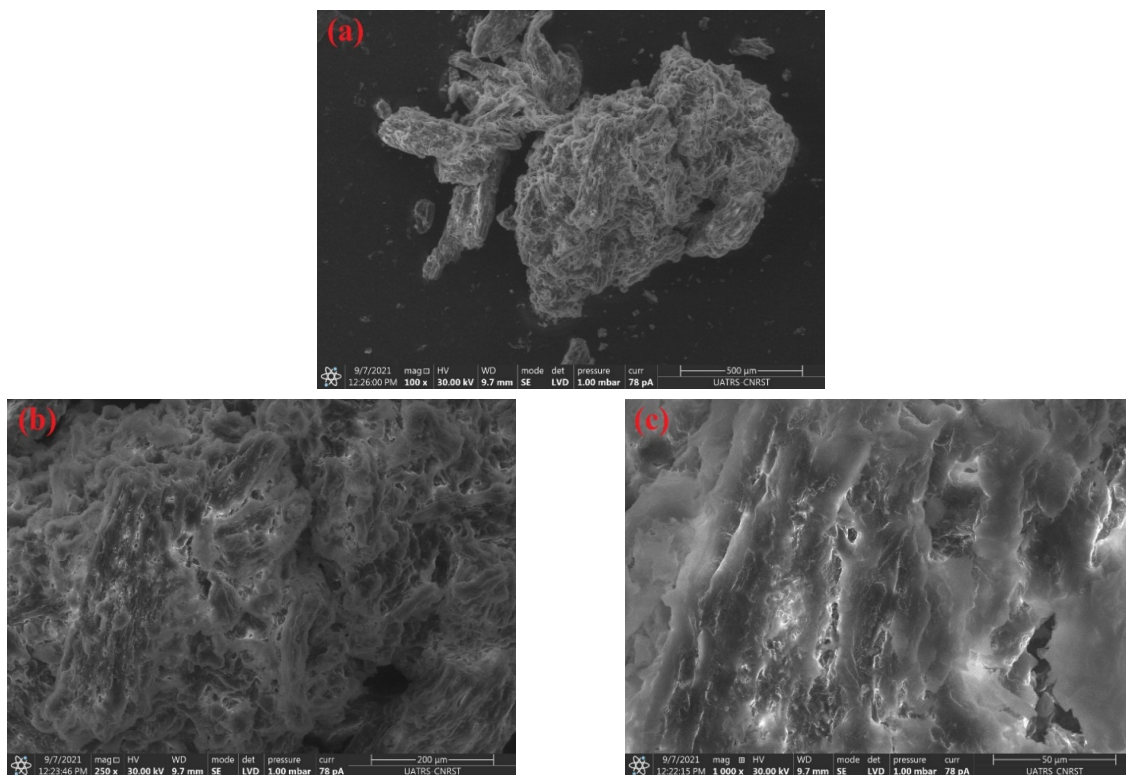


Figure 3: SEM images of lignin scanned at several magnifications (a) $\times 100$, (b) $\times 250$ and (c) $\times 1000$

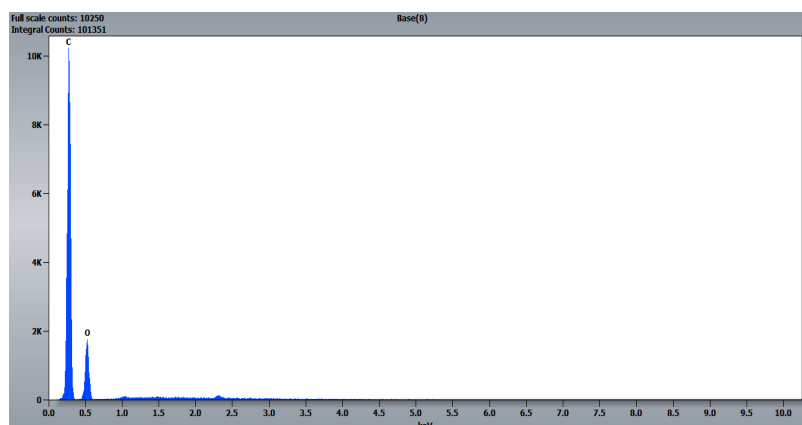


Figure 4: EDX analysis of lignin sample extracted from date seeds

Carbon represents an essential element and principles for the essential structural constituents of lignin, cellulose and hemicelluloses. The greater carbon content of lignin may be related to the number of aromatic carbons from the lignin subunits (*p*-hydroxyphenyl, guaiacyl, and syringyl). Also, the increased purity of extracted lignin can account for its higher carbon concentration.

Thermogravimetric analysis

During the TGA, the weight loss caused by the thermal degradation process of the studied lignin sample was measured as a function of

temperature. The TGA and DTG curves obtained at various heating rates are shown in Figure 5. As shown in the thermogravimetric curve, the thermal degradation of lignin proceeded over a wide temperature range, from approximately 180 to 800 °C.

The weight loss during the first stage of degradation, which occurred between 30 and 100 °C, was less than 5% and was mostly caused by the sample's loss of moisture.³⁸ After the first loss of weight, the degradation process is slower between 110 and 170 °C, when a plateau can be observed. Between 180 and 620 °C, the main thermal degradation for DSL takes place. In this

stage, the primary lignin pyrolysis is shown by a large peak on DTG curves.⁷ Inter-unit linkages are broken down during pyrolytic degradation in this area, which may hasten the degradation process by releasing monomeric phenols into the vapor phase.³⁹

The degradation process may be related to the gradual breakdown of certain aromatic rings in lignin above 500 °C.^{39,40} The solid residue yields are around 40%, which is a significant quantity. This is because highly condensed aromatic structures emerge during this process.³⁹

Differential scanning calorimetry

Figure 6 presents the DSC curve and its derivative for lignin at various heating rates. A strong exothermic peak is visible on each curve, following a broad endothermic dehydration step, as can be seen by examining the DSC plots. These peaks are associated with the light oxidative decomposition of the carbohydrate trace caused by the oxygen content of the sample, which is consistent with what several authors have reported in the literature.⁴¹⁻⁴⁵

Differential scanning calorimetry is the most commonly used technique for determining the glass transition temperature, T_g , of synthetic and natural polymers. The glass transition induces an abrupt change of slope in the DSC thermogram. However, due to the high rigidity of lignin structures, the point at which this change occurs is difficult to observe. In this study, the locally estimated scatterplot smoothing (LOESS) technique was used on the heat flow curve before generating the derivative curves (of the 4 heating rates), using Origin tools. The curves thus obtained were depicted in Figure 6; the glass

transition temperature is taken at the maximum point of the derivative curve.

The observed values of T_g are significantly affected by the heating rate. The glass transition temperature increased with the rising heating rate,⁴⁶ with values ranging from 102.62 to 127.28 °C with the heating rate.

The T_g is the temperature below which amorphous polymers are rigid, there is no overall movement of molecules; while above this temperature, molecules can have an overall movement, so amorphous polymers are fluid or rubbery. The high value obtained in this work can be explained by the aromatic structure, which brings rigidity to the main chain, hydrogen bonding type interactions with water molecules, the high degree of cross-linking and the molecular weight of the lignin investigated.

Kinetic analysis

To determine how the kinetic parameters vary with the conversion, a thermogravimetric study consists of performing a kinetic analysis, which includes weight loss curves obtained at various heating rates 5, 10, 15 and 20 °C/min.

By using isoconversional model-free techniques suggested by FWO, KAS, Kissinger, Tang, MKN, and FR, the activation energy and pre-exponential factor for two degradation steps were calculated. Considering that there are no physical restrictions and that the deterioration of DSL is a global chemical reaction, the mode of degradation is as follows: $f(\alpha) = (1 - \alpha)^n$ with $n = 1$ for FR and $g(\alpha) = -\ln(1 - \alpha)$ for the other approaches. Figure 7 displays the isoconversional lines for each conversion rate.

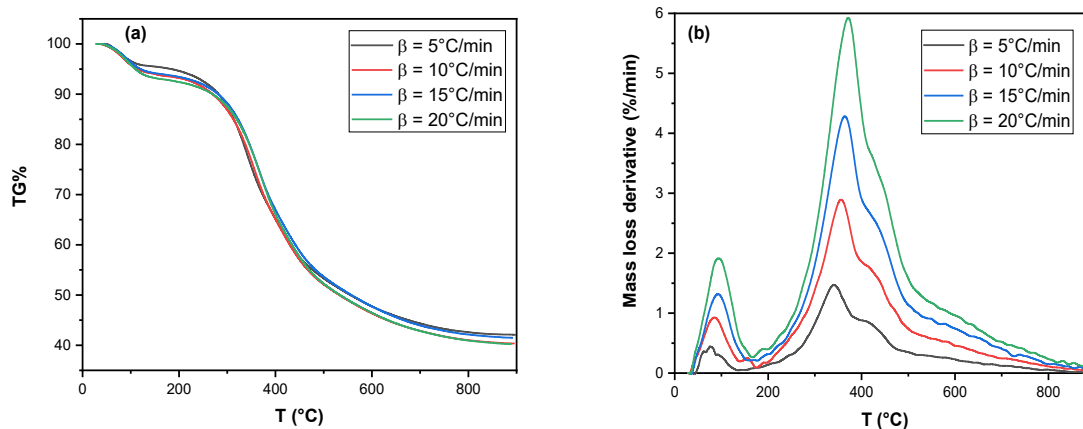


Figure 5: TGA (a) and DTG (b) plots of Klason lignin isolated from date seeds (DSL) at 5, 10, 15, and 20 °C/min

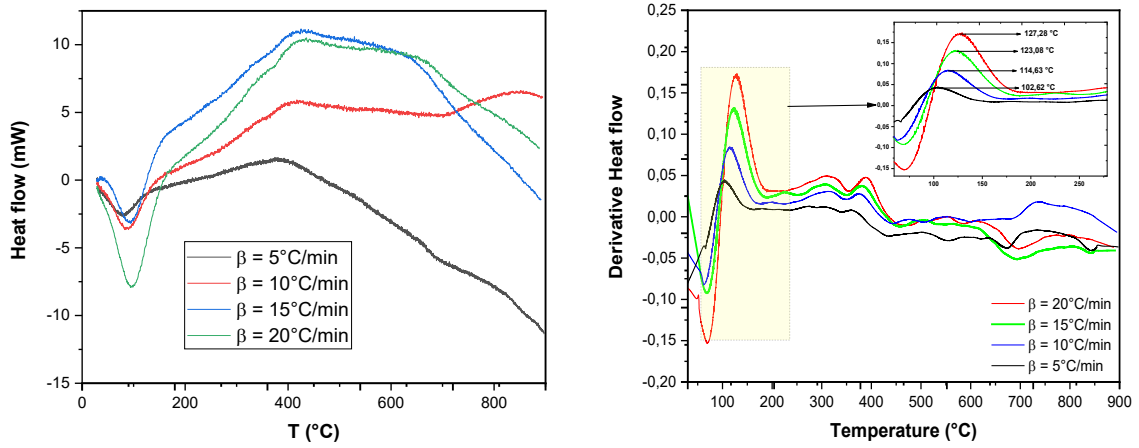


Figure 6: Heat flow and its derivative *versus* temperature plots

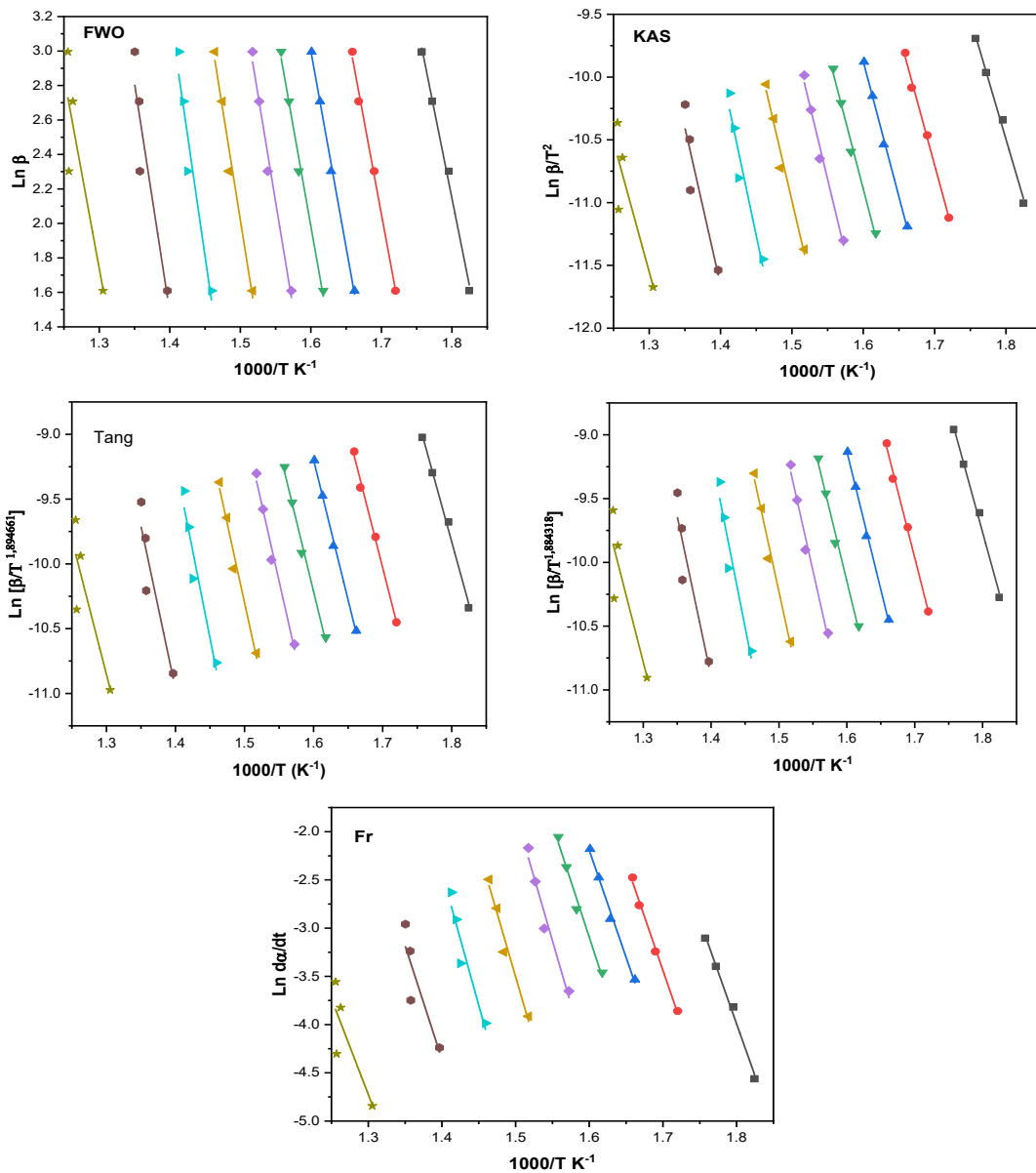


Figure 7: Isoconversional plots of FWO, KAS, Tang, MKN and FR for DSL at various conversion rates

Table 1
Data from Fr, FWO and KAS model-free approaches

Conversion α	FR			FWO			KAS		
	R ²	E _a (kJ.mol ⁻¹)	A (min ⁻¹)	R ²	E _a (kJ.mol ⁻¹)	A (min ⁻¹)	R ²	E _a (kJ.mol ⁻¹)	A (min ⁻¹)
0.1	0.989	161.2	1.34.10 ¹⁵	0.992	161.38	8.62.10 ¹³	0.991	160.50	7.33.10 ¹³
0.2	0.993	174.7	1.01.10 ¹⁵	0.993	174.27	3.20.10 ¹⁴	0.992	173.50	2.83.10 ¹⁴
0.3	0.988	181.06	4.27.10 ¹⁴	0.996	180.06	4.54.10 ¹⁴	0.996	179.24	4.00.10 ¹⁴
0.4	0.977	183.71	1.25.10 ¹⁵	0.988	182.71	3.97.10 ¹⁴	0.986	181.75	3.41.10 ¹⁴
0.5	0.948	196.451	4.65.10 ¹⁶	0.979	196.41	2.67.10 ¹⁵	0.976	195.87	2.51.10 ¹⁵
0.6	0.953	202.8	8.91.10 ¹⁵	0.969	202.73	2.95.10 ¹⁵	0.965	202.13	2.75.10 ¹⁵
0.7	0.874	223.25	1.54.10 ¹⁶	0.911	223.35	3.48.10 ¹⁶	0.902	223.40	3.67.10 ¹⁶
0.8	0.663	208.98	1.39.10 ¹³	0.807	209.88	7.99.10 ¹⁴	0.788	208.70	6.77.10 ¹⁴
0.9	0.539	173.08	1.45.10 ¹⁰	0.659	176.08	4.73.10 ¹¹	0.620	172.26	2.41.10 ¹¹
Average		189.47	8.32.10 ¹⁵		189.65	4.72.10 ¹⁵		188.59	4.86.10 ¹⁵

Table 2
Obtained results from Tang and MKN integral approximation approaches

Conversion α	Tang			MKN		
	R ²	E _a (kJ.mol ⁻¹)	A (min ⁻¹)	R ²	E _a (kJ.mol ⁻¹)	A (min ⁻¹)
0.1	0.991	160.75	8.16.10 ¹³	0.991	160.72	8.04.10 ¹³
0.2	0.992	173.77	3.14.10 ¹⁴	0.992	173.73	3.10.10 ¹⁴
0.3	0.996	179.52	4.44.10 ¹⁴	0.996	179.49	4.38.10 ¹⁴
0.4	0.986	182.04	3.79.10 ¹⁴	0.986	182.01	3.73.10 ¹⁴
0.5	0.977	196.15	2.78.10 ¹⁵	0.977	196.12	2.74.10 ¹⁵
0.6	0.966	202.43	3.05.10 ¹⁵	0.966	202.39	3.00.10 ¹⁵
0.7	0.902	223.69	4.04.10 ¹⁶	0.903	223.64	3.97.10 ¹⁶
0.8	0.789	209.04	7.54.10 ¹⁴	0.789	209.00	7.42.10 ¹⁴
0.9	0.622	172.69	2.76.10 ¹¹	0.622	172.68	2.73.10 ¹¹
Average		188.89	5.35.10 ¹⁵		188.86	5.26.10 ¹⁵

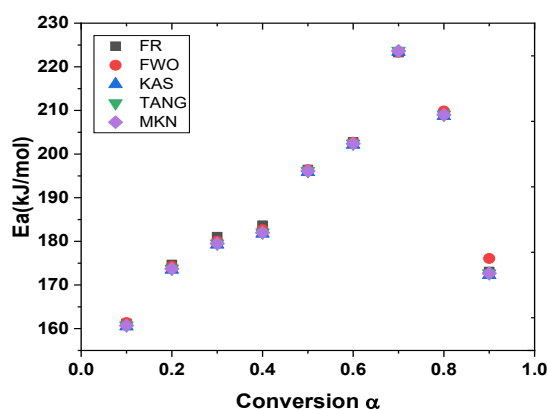


Figure 8: Activation energy as a function of conversion degree α for decomposition of DSL according to FR, FWO, KAS, MKN and Tang approaches

Tables 1 and 2 display the values of E_a and A . Figure 8 depicts the relationship between E_a and conversion rate. From Tables 1 and 2, and Figure 8, it is clear that the apparent value of E_a varies significantly with conversion α , indicating a

complex multi-step degradation of the studied lignin.

The FR, FWO, KAS, MKN and Tang techniques give comparable values of E_a in α range. The apparent activation energy values vary between 160 and 223.7 kJ/mol, for all methods.

The apparent activation energy values found in this study are on par with those in the literature.⁷

The values of E_a and A obtained by Kissinger's approach (Fig. 10, Table 4) are 127 kJ/mol and $4.56 \times 10^{10} \text{ min}^{-1}$, while the same parameters calculated from free model approaches are 160–223 kJ/mol and $4.86 \times 10^{15} \text{ min}^{-1}$ for integral methods, and 161–223.25 kJ/mol and $8.32 \times 10^{15} \text{ min}^{-1}$ for differential Friedman's approach. The results from the first method represented the actual values of kinetic parameters, which are constant throughout the entire pyrolysis process, whereas the results from the second method represented the apparent values of parameters, which are the sum of the physical process and the chemical reaction parameters that take place concurrently during pyrolysis.

Determination of the most probable reaction function

Criado method

The Criado and Coats-Redfern approaches were chosen, since they include the degradation mechanisms to determine the kinetic model of thermal degradation. According to Equation (14), the activation energy (E_a) for every $g(\alpha)$ function can be determined for all heating rates from fitting $\ln(g(\alpha)/T^2)$ versus $1/T$ plots. The E_a and

correlations coefficients (CC) are summarized in Table 3.

According to the Coats Redfern equation, if an appropriate model is chosen for the reaction, the plot of $\ln(g(\alpha)/T^2)$ versus $1/T$ will be linear and will have a high correlation coefficient, in this case, reaction order F2.

One could argue that the dependability of the Coats Redfern method is insufficient and that it cannot be utilized to evaluate reaction kinetics. From this perspective, using the Criado approach is crucial, since it provides us with more information and complements the Coats Redfern method. Figure 9 shows the master curve, which plots $Z(x)/Z(0.5)$ vs α for several mechanisms in accordance with the Criado approach for DSL degradation. These results show that when the experimental master plots were compared to theoretical ones, the kinetic process for the degradation of DSL was most likely described by the reaction order F2. The simplest models are hence reaction order-based models (F_n), which are identical to those used in homogeneous kinetics. The reaction rate in these models is proportional to the concentration, amount, or fraction of reactant that is still presently raised to a specific power, which is the reaction order.

Table 3
Data from Coats-Redfern's method

	E_a (kJ/mol)	A (min^{-1})	Correlation coefficient (CC)
F1	38.97	53.17	0.96
D1	59.53	1090.18	0.88
D2	67.42	3428.97	0.92
D3	52.72	22.67	0.86
D4	101.12	$1.52 \cdot 10^6$	0.98
A2	14.13	0.23	0.92
F0	24.41	1.46	0.83
F2	59.68	6538.36	0.99
R2	34.98	$5.06 \cdot 10^7$	0.86
R3	30.94	3.79	0.91
R4	28.60	2.82	0.88

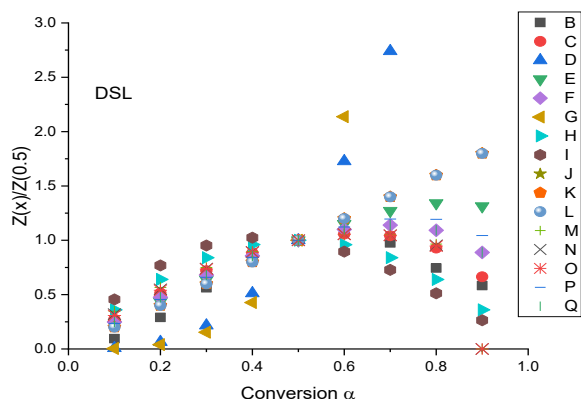


Figure 9: Masterplots of different kinetic models and experimental data at $10\text{ }^{\circ}\text{C}\cdot\text{min}^{-1}$ calculated by Eq. (12) for DSL degradation

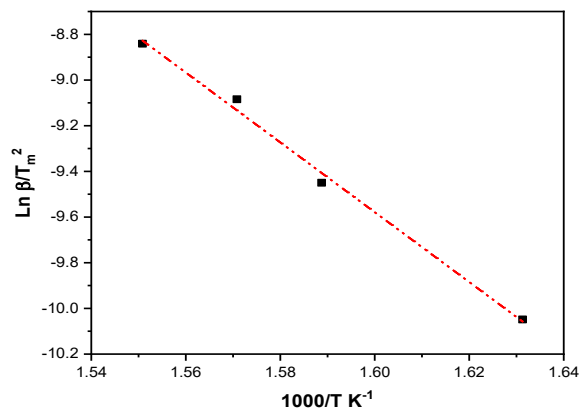


Figure 10: Kissinger's curves of $\text{Ln}(\beta/T^2)$ as a function of $1/T$ for the first and second stages for DSL thermal degradation

Table 4

Thermodynamic parameters of $\Delta S^{\#}$, $\Delta H^{\#}$ and $\Delta G^{\#}$ calculated for thermal degradation of DSL

Parameter	Value
R^2	0.99
Intercept	14.87
Slope	-15.28
E_a ($\text{kJ}\cdot\text{mol}^{-1}$)	126.98
A (min^{-1})	$4.56\cdot 10^{10}$
Average T_p (K)	630.96
$\Delta H^{\#}$ ($\text{Kj}\cdot\text{mol}^{-1}$)	121.74
$\Delta S^{\#}$ ($\text{j}\cdot\text{mol}^{-1}$)	-89.42
$\Delta G^{\#}$ ($\text{Kj}\cdot\text{mol}^{-1}$)	178.17

Thermodynamic parameters

According to data in Table 4, the rise in Gibbs free energy, $\Delta G^{\#}$, indicates that the system's overall energy has increased throughout the thermal degradation process, primarily from heat absorption. It can be inferred from thermodynamic definitions that the degradation reaction is not a spontaneous process. The magnitude of $\Delta G^{\#}$, which indicates how far a reaction is from equilibrium, is also widely recognized. The larger the value of $\Delta G^{\#}$, the further the reaction is from equilibrium and the greater the shift required for the reaction to achieve equilibrium. Table 4 also displays the averaged, $\Delta H^{\#}$, value for the degradation of DSL, representing how significant the energy gap between the activated complex and the reagent is. Obviously, the positive value of $\Delta H^{\#}$ indicates that the related reaction is an endothermic process, which is thermodynamically unfavorable. Moreover, the positive values of entropy $\Delta S^{\#}$ indicate that the activated complexes for DSL had more entropy and a lesser degree of organization than their initial condition. Thereby, a high value of $\Delta S^{\#}$ indicates how far the system is from the

initial equilibrium state to the final thermodynamic equilibrium state.^{27,47-49}

CONCLUSION

The current study has dealt with the extraction of lignin from date seeds using the sulfuric acid process. The lignin was then analyzed through FT-IR and XRD, its thermal properties were observed using TGA and DSC analyses, and its surface morphology was characterized by SEM and EDX analysis. The FT-IR spectra showed homogeneity in the chemical structure of the lignin extracted by sulfuric acid treatments. Lignin was successfully extracted from date seeds using the sulfuric acid process, with an extraction rate that was close to 30% for this substrate. DSC was used to observe the heat of reaction and determine the glass transition temperature of the lignin sample. The lignin sample degraded by an exothermic reaction and was characterized by a glass transition temperature of about $117\text{ }^{\circ}\text{C}$, strongly affected by the heating rate. TGA was used to observe the thermal degradation of the biomaterial. The extracted lignin was found thermally stable, with higher char yield of about

40%. Several methods were used to derive kinetic parameters. The isoconversional techniques provide comparable values of E_a in α range, demonstrating the suitability of using these methods to derive the kinetic parameters. Using the Criado method, the most probable reaction function of DSL degradation was determined and was described by the reaction order F2.

REFERENCES

- ¹ N. Assoumani, M. Simo-Tagne, F. Kifani-Sahban, A. T. Tagne, M. El. Marouani *et al.*, *Sustainability*, **13**, 24 (2021), <https://doi.org/10.3390/su132413892>
- ² B. Lucia, F. Cotana, E. Fortunati and J. M. Kenny, *Carbohydr. Polym.*, **94**, 154 (2013), <https://doi.org/10.1016/j.carbpol.2013.01.033>
- ³ L. Hu, H. Pan, Y. Zhou and M. Zhang, *BioResources*, **6**, 3515 (2011), <https://doi.org/10.15376/biores.6.3.3515-3525>
- ⁴ S. H. Lee, T. V. Doherty, R. J. Linhardt and J. S. Dordick, *Biotechnol. Bioeng.*, **102**, 1368 (2009), <https://doi.org/10.1002/bit.22179>
- ⁵ N. Brosse, M. N. M. Ibrahim and A. A. Rahim, *Int. Sch. Res. Notices*, **2011**, ID 461482 (2011), <https://doi.org/10.5402/2011/461482>
- ⁶ F. E. Barton, *Anim. Feed Sci. Technol.*, **21**, 279 (1988), [https://doi.org/10.1016/0377-8401\(88\)90107-1](https://doi.org/10.1016/0377-8401(88)90107-1)
- ⁷ G. Jiang, D. J. Nowakowski and A. V. Bridgwater, *Thermochim. Acta*, **498**, 61 (2010), <https://doi.org/10.1016/j.tca.2009.10.003>
- ⁸ M. Brebu and C. Vasile, *Cellulose Chem. Technol.*, **44**, 353 (2010), [https://www.cellulosechemtechnol.ro/pdf/CCT9\(2010\)/P.353-363.pdf](https://www.cellulosechemtechnol.ro/pdf/CCT9(2010)/P.353-363.pdf)
- ⁹ M. Wang, M. Leitch and C. Xu, *Eur. Polym. J.*, **45**, 3380 (2009), <https://doi.org/10.1016/j.eurpolymj.2009.10.003>
- ¹⁰ M. Sneha, C. Archana and I. Soni, *Int. J. Knowl. Eng.*, **3**, 11 (2012)
- ¹¹ H. El Abbari, S. Bentahar, M. El Marouani, M. Taibi, A. Zerriouh *et al.*, *J. Therm. Anal. Calorim.*, **137**, 1485 (2019), <https://doi.org/10.1007/s10973-019-08060-8>
- ¹² J. Domínguez, M. Oliet, M. Alonso, M. Gilarranz and F. Rodríguez, *Ind. Crop. Prod.*, **27**, 150 (2008), <https://doi.org/10.1016/j.indcrop.2007.07.006>
- ¹³ D. Ferdous, A. K. Dalai, S. K. Bej and R. W. Thring, *Energ. Fuel.*, **16**, 1405 (2002), <https://doi.org/10.1021/ef0200323>
- ¹⁴ A. Sluiter, B. Hames, R. Ruiz, C. Scarlata, J. Sluiter *et al.*, *Laboratory Analytical Procedure*, Colorado, 2008, <https://www.nrel.gov/docs/gen/fy13/42618.pdf>
- ¹⁵ M. Saber, L. El Hamdaoui, M. El Moussaouiti and M. Tabyaoui, *Cellulose Chem. Technol.*, **56**, 69 (2022), <https://doi.org/10.35812/CelluloseChemTechnol.2022.56.06>
- ¹⁶ M. E. Brown, M. Maciejewski, S. Vyazovkin, R. Nomen, J. Sempere *et al.*, *Thermochim. Acta*, **355**, 125 (2000), [https://doi.org/10.1016/S0040-6031\(00\)00443-3](https://doi.org/10.1016/S0040-6031(00)00443-3)
- ¹⁷ H. L. Friedman, *J. Polym. Sci., Part C: Polym. Symp.*, **6**, 183 (1964), <https://doi.org/10.1002/polc.5070060121>
- ¹⁸ J. H. Flynn and L. A. Wall, *J. Res. A Phys. Chem.*, **70**, 487 (1966), <http://dx.doi.org/10.6028/jres.070A.043>
- ¹⁹ T. Ozawa, *Bull. Chem. Soc. Jpn.*, **38**, 1881 (1965), <http://dx.doi.org/10.1246/bcsj.38.1881>
- ²⁰ H. E. Kissinger, *J. Res. Technol.*, **57**, 14 (1956), <http://dx.doi.org/10.6028/jres.057.026>
- ²¹ T. Akahira and T. Sunose, *Sci. Technol.*, **16**, 22 (1971), [https://www.scirp.org/\(S\(351jmbntvnsjt1aadkpozsj\)\)/reference/ReferencesPapers.aspx?ReferenceID=118643](https://www.scirp.org/(S(351jmbntvnsjt1aadkpozsj))/reference/ReferencesPapers.aspx?ReferenceID=118643)
- ²² A. W. Coats and J. P. Redfern, *Nature*, **201**, 68 (1964), <https://doi.org/10.1038/201068a0>
- ²³ P. Madhysudanan, K. Krishnan and K. Ninan, *Thermochim. Acta*, **221**, 13 (1993), [https://doi.org/10.1016/0040-6031\(93\)80519-G](https://doi.org/10.1016/0040-6031(93)80519-G)
- ²⁴ W. Tang, Y. Liu, H. Zhang and C. Wang, *Thermochim. Acta*, **408**, 39 (2003), [https://doi.org/10.1016/S0040-6031\(03\)00310-1](https://doi.org/10.1016/S0040-6031(03)00310-1)
- ²⁵ J. M. Criado, *Thermochim. Acta*, **24**, 186 (1978), [https://doi.org/10.1016/0040-6031\(78\)85151-X](https://doi.org/10.1016/0040-6031(78)85151-X)
- ²⁶ J. J. Rooney, *J. Mol. Catal. A Chem.*, **96**, L1 (1995), [https://doi.org/10.1016/1381-1169\(94\)00054-9](https://doi.org/10.1016/1381-1169(94)00054-9)
- ²⁷ L. T. Vlaev, V. G. Georgieva and M. P. Tavlieva, in “Reactions and Mechanisms in Thermal Analysis of Advanced Materials”, edited by T. Atul and R. Baldev, Wiley, 2015, p. 547, <https://doi.org/10.1002/9781119117711.ch22>
- ²⁸ A. Mandal and D. Chakrabarty, *Carbohydr. Polym.*, **86**, 1291 (2011), <https://doi.org/10.1016/j.carbpol.2011.06.030>
- ²⁹ P. N. Hasegawa, A. F. D. Faria, A. Z. Mercadante, E. A. Chagas, R. Pio *et al.*, *Food Sci. Technol.*, **30**, 552 (2010), <https://doi.org/10.1590/S0101-20612010000200040>
- ³⁰ R. M. Silverstein, F. X. Webster, D. J. Kiemle, D. L. Bryce and V. Lafond, “Identification spectrométrique de composés organiques”, 2nd ed., De Boeck, 2007
- ³¹ T. You and F. Xu, in “Applications of Molecular Spectroscopy to Current Research in the Chemical and Biological Sciences”, edited by M. T. Stauffer, IntechOpen, 2016, p. 235, <https://doi.org/10.5772/64581>
- ³² B. Ahvazi, É. Cloutier, O. Wojciechowicz and T.-D. Ngo, *ACS Sustain. Chem. Eng.*, **4**, 5090 (2016), <https://doi.org/10.1021/acssuschemeng.6b00873>
- ³³ O. Faix and O. Beinhoff, *J. Wood Chem. Technol.*, **8**, 505 (1988), <https://doi.org/10.1080/02773818808070698>
- ³⁴ U. Kües, “Wood Production, Wood Technology, and Biotechnological Impacts”, Universitätsverlag

Göttingen, 2007, <https://doi.org/10.17875/gup2007-262>

³⁵ L. El Hamdaoui, M. El Moussaouiti and S. Gmouh, *Polym. Bull.*, **72**, 3031 (2015), <http://dx.doi.org/10.1007%2Fs00289-015-1451-z>

³⁶ A. Goudarzi, L.-T. Lin and F. K. Ko, *J. Nanotechnol. Eng. Med.*, **5**, 021006 (2014), <https://doi.org/10.1115/1.4028300>

³⁷ S. Kubo and J. Kadla, *J. Polym. Environ.*, **13**, 97 (2005), <https://doi.org/10.1007/s10924-005-2941-0>

³⁸ M. Poletto, A. J. Zattera and R. M. Santana, *Bioresour. Technol.*, **126**, 7 (2012), <https://doi.org/10.1016/j.biortech.2012.08.133>

³⁹ A. Tejado, C. Peña, J. Labidi, J. M. Echeverria and I. Mondragon, *Bioresour. Technol.*, **98**, 1655 (2007), <https://doi.org/10.1016/j.biortech.2006.05.042>

⁴⁰ X. Zhao and D. Liu, *Ind. Crop. Prod.*, **32**, 284 (2010), <https://doi.org/10.1016/j.indcrop.2010.05.003>

⁴¹ H. Yang, R. Yan, H. Chen, D. H. Lee and C. Zheng, *Fuel*, **86**, 1781 (2007), <https://doi.org/10.1016/j.fuel.2006.12.013>

⁴² J. Lisperguer and P. Perez, *J. Chil. Chem. Soc.*, **54**, 460 (2009), <http://dx.doi.org/10.4067/S0717-97072009000400030>

⁴³ H. Haykiri-Acma, S. Yaman and S. Kucukbayrak, *Fuel Process. Technol.*, **91**, 759 (2010), <https://doi.org/10.1016/j.fuproc.2010.02.009>

⁴⁴ Y. Liu, T. Hu, Z. Wu, G. Zeng, D. Huang *et al.*, *Environ. Sci. Pollut. Res.*, **21**, 14004 (2014), <https://doi.org/10.1007/s11356-014-3342-5>

⁴⁵ M. E. Vallejos, F. E. Felissia, A. A. Curvelo, M. D. Zambon, L. E. Ramos *et al.*, *Bioresources*, **6**, 1158 (2011), <https://doi.org/10.15376/biores.6.2.1158-1171>

⁴⁶ M. Poletto, *Maderas: Ciênc. Tecnol.*, **19**, 11 (2017), <http://dx.doi.org/10.4067/S0718-221X2017005000006>

⁴⁷ V. Georgieva, D. Zvezdova and L. Vlaev, *Chem. Cent. J.*, **6**, 11 (2012), <https://doi.org/10.1186/1752-153X-6-81>

⁴⁸ Y. Hao, X. Fan, Z. Huang, Y. Li, Q. Ye *et al.*, *J. Therm. Anal. Calorim.*, **128**, 1077 (2016), <https://doi.org/10.1007/s10973-016-5972-y>

⁴⁹ E. Taboada, G. Cabrera, R. Jiménez and G. Cardenas, *J. Appl. Polym. Sci.*, **114**, 2043 (2009), <https://doi.org/10.1002/app.30796>